HHS Public Access

Author manuscript

J Am Chem Soc. Author manuscript; available in PMC 2014 December 11.

Published in final edited form as:

J Am Chem Soc. 2013 December 11; 135(49): 18536–18548. doi:10.1021/ja4086758.

On the Dynamic Stoichiometry of Metal Chalcogenide Nanocrystals: Spectroscopic Studies of Metal Carboxylate Binding and Displacement

Nicholas C. Anderson, **Mark P. Hendricks**, **Joshua J. Choi**, and **Jonathan S. Owen***

Department of Chemistry, Columbia University, 3000 Broadway, MC 3121, New York, NY 10027.

Abstract

We demonstrate that metal carboxylate complexes (L–M(O_2CR)$_2$, R = oleyl, tetradecyl, M = Cd, Pb) are readily displaced from carboxylate-terminated ME nanocrystals (ME = CdSe, CdS, PbSe, PbS) by various Lewis bases (L = tri-*n*-butylamine, tetrahydrofuran, tetradecanol, N,N-dimethyl-*n*-butylamine, tri-*n*-butylphosphine, N,N,N',N'-tetramethylbutylene-1,4-diamine, pyridine, N,N,N',N'-tetramethylethylene-1,2-diamine, *n*-octylamine). The relative displacement potency is measured by ^{1}H NMR spectroscopy and depends most strongly on geometric factors like sterics and chelation, though also on the hard/soft match with the cadmium ion. The results suggest that ligands displace L–M(O_2CR)$_2$ by cooperatively complexing the displaced metal ion as well as the nanocrystal. Removal of up to 90% of surface bound Cd(O_2CR)$_2$ from CdSe and CdS nanocrystals decreases the Cd:Se ratio from 1.1 ± 0.06 to 1.0 ± 0.05, broadens the $1S_e$-$2S_{3/2h}$ absorption and decreases the photoluminescence quantum yield (PLQY) from 10% to <1% (CdSe) and 20% to <1% (CdS). These changes are partially reversed upon rebinding of M(O_2CR)$_2$ at room temperature (~60 %) and fully reversed at elevated temperature. A model is proposed where electron accepting M(O_2CR)$_2$ complexes (Z-type ligands) reversibly bind to nanocrystals leading to a range of stoichiometries for a given core size. The results demonstrate that nanocrystals lack a single chemical formula, but are instead dynamic structures with concentration-dependent compositions. The importance of these findings to the synthesis and purification of nanocrystals as well as ligand exchange reactions is discussed.

Keywords

CdSe; CdS; PbS; PbSe; nanocrystals; quantum dots; ligand exchange; stoichiometry; quantum yield

*jso2115@columbia.edu.

SUPPORTING INFORMATION ^{1}H NMR spectra used for Table 1, additional characterization of L-M(O_2CR)$_2$, UV-Visible absorption spectra, photoluminescence spectra, and vinyl ^{1}H NMR spectra used for Figure 4, RBS data, temperature and solvent dependent ^{1}H NMR spectra, and changes in the UV-vis and PLQY spectra with added CdX_2 along with TEM, dynamic light scattering analysis, and optical spectra for lead chalcogenide nanocrystals are included free of charge via the Internet at http://pubs.acs.org.

Introduction

Manipulating nanocrystal surface ligands is a crucial step in the conversion of these tunable materials into optoelectronic devices and fluorescent labels for biological imaging.[1-8] Ligand exchange is required to remove organic surfactants and allow charge transport in nanocrystal solids as well as to prepare water-soluble nanocrystals that target specific cellular sites. These manipulations also influence surface trap states and thereby control photoluminescence quantum yield (PLQY).[9-27] As a result, detailed studies have appeared that seek to understand the relationship between ligation and charge trapping.[6,28-40] However, models that adequately explain this behavior are lacking, and the precise relationship between PLQY and ligation largely remains a mystery.

Many studies conclude that the nature of the ligand shell depends on the stoichiometry of the nanocrystals. Colloidal synthesis often affords nanocrystals rich in metal cations whose charge neutrality is maintained by anionic X-type ligands (Scheme 1).[17,32,33,41-46] This charge neutrality has been demonstrated in several studies where proton transfer[17,32,33,43,47] or trimethylsilyl transfer is required to mediate ligand exchange (Scheme 2).[43,45,48] Metal-enrichment is also known to increase with decreasing nanocrystal size, a finding that supports the growing consensus that metal-enrichment occurs at surfaces.[34,49-51] Thus metal chalcogenide nanocrystals are thought to be a stoichiometric core with a layer of metal-ligand complexes adsorbed to their surfaces.[17,32,33,43] However, the precise stoichiometry appears to vary depending on the synthesis and isolation procedure, and the range over which stoichiometry can vary for a given size is unclear. [34,49-52]

Changes to nanocrystal stoichiometry are known to influence optoelectronic properties such as PLQY and electrical transport.[41,44,53-56] For example, charge carrier concentrations in nanocrystal thin-films can be systematically altered by changing stoichiometry with physical vapor deposition[57] or wet chemical methods.[34,56,58-61] PLQY also depends on stoichiometry, as observed in successive ionic layer adsorption and reaction (SILAR) studies, where cadmium chalcogenide nanocrystals with cadmium-rich surface layers are generally brighter than chalcogenide-rich nanocrystals.[62-67] In addition, several others have shown that exchanging native metal ions with a “foreign” metal, such as Cd^{2+} for Pb^{2+} at lead chalcogenide nanocrystal surfaces can increase PLQY,[21,27,68-72] prevent photoionization,[73,74] and increase charge carrier mobilities (Z-type exchange, Scheme 2).[53,75,76] Thus passivation of surface chalcogen sites can be accomplished with a layer of bound M^{2+} ions. Although it has been suggested that phosphine ligands may also passivate surface chalcogenide sites, the ^{31}P NMR evidence supporting this conclusion is controversial.[18,19,77-79] Neutral donors such as phosphines can bind to metal centers thereby destabilizing their low lying vacant orbitals,[10,25,26,45] however passivation of high-lying filled orbitals on surface chalcogenide sites is only in principle possible with acceptor ligands, such as Lewis acidic cadmium centers. These results suggest that surfaces rich in metal ions are important to prevent charge trapping and that control over nanocrystal stoichiometry is key to optimizing their PLQY.[41]

In this study we demonstrate that the surface layer of excess metal ions are labile and reversibly bind to and dissociate from nanocrystal surfaces as carboxylate complexes

($M(O_2CR)_2$); denoted as a Z-type ligand. According to the covalent bond classification method developed by M. L. H. Green, L-type ligands are two-electron donors (neutral Lewis bases, dative covalent bonds), X-type ligands are one-electron donors (anionic, normal covalent bonds), and Z-type ligands are two-electron acceptors (Lewis acids) (Scheme 1).[80] We show that L-type donors, often used in nanocrystal isolation and ligand-exchange procedures (Scheme 2), displace metal carboxylate complexes ($L–M(O_2CR)_2$) (Scheme 3). Furthermore, displacement is reversible, occurs rapidly at room temperature, and depends on the solution concentration of L-type donors that competitively bind $M(O_2CR)_2$ as well as the nanocrystal surface. We also show that the $M(O_2CR)_2$ surface coverage has a positive, super-linear correlation with the PLQY. Photoluminescence is very sensitive to coverage between 2 - 3 carboxylates/nm^2, corresponding to Cd:Se ratios of 1.2 - 1.1, a range of stoichiometry that is commonly obtained in other syntheses,[17,42,45,50,81] and is near zero below 2 carboxylates/nm^2. These observations indicate that nanocrystal stoichiometry can vary for a given core size, and that careful maintenance of nanocrystal stoichiometry is crucial in order to systematically control and understand nanocrystal optoelectronic behavior. Together these experiments elucidate a novel type of surface reactivity that can be used to explain the majority of ligand exchange reactions reported previously, as well as their effect on nanocrystal PLQY.

Results and Discussion

Monitoring Z-type Displacement with ^{1}H NMR Spectroscopy

Displacement of cadmium carboxylate from cadmium selenide nanocrystals (d = 3.3 - 3.7 nm) was monitored *in situ* using ^{1}H NMR spectroscopy. The vinylic hydrogens of surface-bound oleyl chains display a broad resonance in the range 5.3 – 5.6 ppm, well separated from other ligand-derived signals and therefore useful for monitoring displacement reactions (Figure 1). The NMR line-width provides a convenient method to distinguish bound ligands, which tumble slowly and have broad signals, from ligands moving freely in solution, which display sharp signals.[17,32,33,42,43,82] In this way, NMR spectroscopy can be used to study nanocrystals in the presence of small molecule impurities, especially unconverted $M(O_2CR)_2$ remaining from the synthesis, as well as to determine the surface coverage of carboxylate ligands (see experimental). Using this approach we obtained isolated nanocrystals for this study with 3.3 - 3.7 carboxylates/nm^2, coverages similar to those reported previously.[17,32,45,83]

Displacement of cadmium carboxylate from these nanocrystals was observed in the presence of several L-type Lewis bases including alcohols, amines, and phosphines. For example, adding N,N,N',N'-tetramethylethylene-1,2-diamine (TMEDA) to the nanocrystals displaces a carboxyl fragment with a sharp vinyl resonance that shifts up-field and increases in intensity if additional TMEDA is added (Figure 1). While in principle this result can be explained by simple displacement of the carboxylate ligands, this would require that the anionic charge of the carboxylate is seperated from the positively-charged surface-bound cation. Instead, we hypothesized that the “free” carboxyl fragment is derived from a TMEDA-bound cadmium carboxylate complex displaced from the surface of the nanocrystal. A similar reaction pathway has been previously suggested to explain the

displacement of surfactant ligands with hydrazine, diamines,[84] phosphines, and primary amines[85] but never explicitely demonstrated.

Isolation and Characterization of L-Cd(O_2CR)$_2$

To confirm our hypothesis the nanocrystals were separated by precipitation with methyl acetate and the supernatant analyzed (see experimental section). Upon drying under vacuum, a nearly colorless oil was obtained that showed sharp ^{1}H NMR signals from aliphatic and vinylic hydrogens characteristic of carboxyl fragments as well as cadmium-bound TMEDA ligands which are shifted slightly up-field from the frequencies of free TMEDA (~ 2:1 carboxyl:TMEDA). In addition, a broad feature of low intensity is visible at δ = 9.3 ppm that we assign to the acidic hydrogen of a carboxylic acid present in lower concentration (8 ± 3%) (Figure S1). A strong asymmetric stretching band from the cadmium-bound carboxylate (ν_{assym}(O_2CR) = 1560 cm^{-1}) is visible in the FT-IR spectrum that matches an independently prepared sample of (κ^2-TMEDA)Cd(O_2CR)$_2$ and is readily distinguished from the signals of oleic acid mixed with TMEDA (ν(HO_2CR) = 1720 cm^{-1}) (Figure S2).

To provide further support for Cd(O_2CR)$_2$ removal, we studied Cd(O_2CR)$_2$ displacement in the presence of tri-*n*-butylphosphine (Bu_3P) with the help of ^{31}P NMR spectroscopy. Much like TMEDA, adding Bu_3P to the nanocrystals causes new carboxyl resonances to appear in the ^{1}H NMR spectrum including one in the vinyl region that shifts up-field, sharpens, and increases in intensity when additional Bu_3P is added (Figure S3). (Bu_3P)Cd(O_2CR)$_2$ was isolated from the supernatant and identified with both ^{1}H and ^{31}P NMR spectroscopies, including a diagnostic ^{31}P NMR signal that matched an independently prepared sample (Figure 2, Figure S4). X-ray photoelectron spectroscopy of the isolated byproduct shows signals expected for (Bu_3P)Cd(O_2CR)$_2$ with no detectable signals in the range expected for Se (Figure 2), evidence that etching of the CdSe core is not the source of cadmium.[20,36,86-88]

Generality of Z-type Displacement Reactivity

To investigate the generality of this reaction in other materials, a solution of zincblende cadmium sulfide nanocrystals with tetradecanoate ligands was mixed with TMEDA. Rapid displacement of (κ^2-TMEDA)Cd(O_2CR)$_2$ (R = tridecyl) was observed by ^{1}H NMR spectroscopy (Figure S5). TMEDA also displaces a (κ^2-TMEDA)Pb(O_2CR)$_2$ (R = oleyl) complex from PbS and PbSe nanocrystals without etching the nanocrystal cores, a result that was confirmed by comparing ^{1}H NMR, FT-IR, and electron-dispersive X-ray spectra of the soluble byproduct with those of an independently synthesized sample (Figures S6). *In situ* ^{1}H NMR spectra taken upon adding TMEDA to PbS and PbSe nanocrystals showed a similar appearance of free oleyl chains as observed for CdSe. However, TMEDA proved to be less effective for displacing M(O_2CR)$_2$ from PbS and PbSe nanocrystals than from CdSe nanocrystals, a property that likely derives from the partially occupied valence shell of the Pb^{2+} ion (Figures S7 and S8).

Having established that the removal of M(O_2CR)$_2$ using TMEDA is general for several classes of nanocrystals, we returned to cadmium selenide to measure the relative Z-type displacement potencies of L-type ligands *in situ* using ^{1}H NMR spectroscopy (Scheme 4). Among those studied, primary amines and TMEDA displace the greatest proportion of

$Cd(O_2CR)_2$ (95 ± 10%, 2.0 M), while pyridine and Bu_3P displace a moderate amount (35 - 40 ± 5%, 2.0 M). Common anti-solvents used in nanocrystal purification, such as acetone, methyl acetate, and acetonitrile, do not displace significant amounts of L–$Cd(O_2CR)_2$, while high concentrations (2.0 M) of primary alcohols displace ~10% of the starting $Cd(O_2CR)_2$. This difference is not the result of a change in solvent dielectric; displacement with pyridine occurs to the same extent in d_6-benzene and d_2-methylene chloride (Figure S9). Related studies on the reaction of cadmium selenide nanocrystals with methanol propose that carboxylate ligands are displaced by proton-mediated X-type exchange without releasing Cd^{2+} (Scheme 2)[32,33,47] and leaving a surface bound methoxide.[17] However, under our conditions 80 mg of nearly colorless $(CH_3OH)_n$•$Cd(O_2CR)_2$ was isolated from 1.86 g of nanocrystals (10% yield of total $Cd(O_2CR)_2$) upon precipitation with pure methanol, that was characterized unambiguously with ^{1}H NMR and FT-IR spectroscopies (Figure S10).

Steric and Electronic Effects

The relative potency of the Lewis bases shown in Scheme 4 illustrates several features of the Z-type displacement reaction. First, electronic effects are important as Bu_3P is more effective than tri-*n*-butylamine (Bu_3N), and primary amines are more effective than primary alcohols, presumably because they are more polarizable and electron rich, respectively, making them a better match for the soft, Lewis acidic cadmium ion. Second, chelation plays an important role, making TMEDA among the most effective displacement reagents while N,N-dimethyl-*n*-butylamine (Me_2NBu) is among the weakest. Chelation also explains why TMEDA is significantly more potent than N,N,N',N'-tetramethylbutylene-1,4-diamine, a result that is expected from the relative stability of the five membered ring formed in (κ^2-TMEDA)$Cd(O_2CR)_2$ compared with the analogous seven membered ring in (κ^2-N,N,N',N'-tetramethylbutylene-1,4-diamine)$Cd(O_2CR)_2$.[89] Finally, the steric profile of the incoming ligand has a significant impact on its displacement potency. Steric effects explain the large differences between Bu_3N, Me_2NBu, and *n*-butylamine, given their similar pK_bs.[90] Likewise, the relatively small steric profile of pyridine enables $Cd(O_2CR)_2$ removal, the potency of which is otherwise difficult to explain given its weaker basicity and hard/soft match with the cadmium center.

The sensitivity to sterics is intriguing and implies that displacement of $Cd(O_2CR)_2$ may be promoted by cooperative binding of the L-type ligand to nanocrystal surface where steric effects are known to strongly influence binding affinity.[18,45] In the case of primary amines, displacement is accompanied by binding of the L-type ligand to the surface of the nanocrystal, dramatically increasing the PLQY (see discussion below) and maintaining the nanocrystals solubility even after > 90% of the $Cd(O_2CR)_2$ has been displaced. On the other hand, displacing a similar amount of $Cd(O_2CR)_2$ using TMEDA causes precipitation. Presumably any bound TMEDA does not provide enough steric repulsion to maintain the solubility. On the basis of these observations, we conclude that the displacement reaction can be a cooperative process in cases where the added ligand binds both the nanocrystal surface and the displaced $Cd(O_2CR)_2$. In particular, ligands with a small steric profile, like pyridine and *n*-alkylamines, may drive the displacement equilibrium by binding the nanocrystal.

Displacement Kinetics

Having shown that a variety of ligands displace L–$Cd(O_2CR)_2$ from CdSe nanocrystals, we investigated the kinetics of the displacement reaction. *In situ* ^{1}H NMR measurements indicate that displacement is nearly complete (> 90%) within a few minutes of mixing TMEDA with nanocrystals in benzene. The initially rapid displacement is followed by a slower reaction that liberates a much smaller portion of (κ^2-TMEDA)$Cd(O_2CR)_2$, however, the total change observed after the rapid initial reaction is small and near the estimated uncertainty of the NMR measurement (Figure 3). Surprisingly, the reaction rapidly reaches equilibrium, even under conditions where the majority of surface cadmium atoms are displaced. The fast kinetics indicate that nanocrystal stoichiometry is very sensitive to the presence of Lewis bases and is easily altered. Furthermore, these observations indicate that the relative extent of displacement shown in Scheme 4 reflects an equilibrium condition rather than differences in reaction rate. In support of this conclusion, we analyzed a mixture of pyridine and nanocrystals before and after heating to 100 °C for 6 hours and found no measurable change to the final ratio of bound and free $Cd(O_2CR)_2$ (Figure S11).

Knowing that TMEDA and primary amines are the most potent $Cd(O_2CR)_2$ displacement reagents and that the displacement reaction establishes equilibrium quickly, we attempted to isolate nanocrystals with a minimal $Cd(O_2CR)_2$ coverage. We hypothesized that the chelation ability of TMEDA coupled with the cooperative binding of primary amines might allow access to even lower coverages than either L-type ligand alone. Soluble nanocrystals with *n*-octylamine ligands (d = 3.5 nm, ~170 *n*-octylamine ligands, 4.5 ligands nm^{-2}, Table 1, Figure S12) could be obtained by displacing $Cd(O_2CR)_2$ with a 50:50 mixture of TMEDA and *n*-octylamine (see experimental section). However, ^{1}H NMR spectroscopy of nanocrystals isolated from this solution shows that 6% of the bound carboxyl ligands remain, a decrease from 160 per nanocrystal (4.2 nm^{-2}) to 10 per nanocrystal (0.3 nm^{-2}). No signals from TMEDA are visible in the ^{1}H NMR spectrum, presumably because primary amines preferentially bind the nanocrystal surface. The stoichiometry of the isolated nanocrystals was analyzed with Rutherford backscattering spectrometry, verifying that the Cd:Se ratio decreases from 1.10 ± 0.06 to 1.01 ± 0.05 after exposure to TMEDA (Figure S13). Repeated treatments with amine and TMEDA mixtures did not further reduce the carboxylate loading, and nanocrystals always retained a carboxylate coverage of at least 0.3 nm^{-2}. Similar difficulty was previously reported when removing native ligands using pyridine and other neutral donors, though the origins of this coverage dependent binding affinity remain are uncertain.[19,31,87,91] While it is natural to suppose that a mixture of surface sites with different binding affinities results in some ligands being bound more tightly, this behavior may also result from allosteric electronic effects associated with forming the complete polar facets of a stoichiometric nanocrystal.

Reversibility of Displacement

The concentration dependence of the $Cd(O_2CR)_2$ coverage and the rapid displacement kinetics suggest that rebinding may be equally facile. To investigate the reversibility of displacement, a solution of unaggregated nanocrystals with a low surface $Cd(O_2CR)_2$ coverage (0.6 carboxylates/nm^2) was stirred with anhydrous cadmium oleate at room temperature in toluene (see experimental section). After separating free $Cd(O_2CR)_2$ by

repeated precipitation of the nanocrystals with methyl acetate, the carboxylate coverage had increased to 2.1 nm^{-2}, roughly 60% of the coverage prior to displacement with TMEDA (Figure S14). Similar results were obtained with CdS nanocrystals (see below). The partial rebinding at room temperature may result from slow organization of carboxylate ligands at high coverages or a slow surface reconstruction that must be reversed prior to rebinding. However, complete recovery of the original surface ligand density (3.1 nm^{-2}) could be achieved by heating the nanocrystals to 240° C under nitrogen in the presence of cadmium oleate and oleic acid. Under these conditions the nanocrystals grow slightly (d = 3.6 to 3.8 nm) as measured by the small red-shift in their UV-visible absorption spectrum (7 nm), which we attribute to Ostwald ripening given that no selenium precursor was added (Figure 5). While the temperature dependence of binding deserves further study, the reversibility implies that surface-bound cadmium ions are in equilibrium with free cadmium complexes in solution, and thus nanocrystal stoichiometry is concentration dependent.

While nanocrystals with ligand coverages of ~3 carboxylates/nm^2 were chosen for this study on the basis of a ^{1}H NMR spectrum that lacked the sharp signals from free carboxyl fragments, a number of observations suggest that higher coverages are possible. First, the density of atoms on common facets of CdSe nanocrystals is greater than 3 nm^{-2} (CdSe (111) = 6.2 atoms/nm^2 and (100) = 5.4 atoms/nm^{-2}). Assuming that a maximum of one excess cadmium can bind each surface selenium atom of a cubeoctahedral nanocrystal with equal area (111) and (100) facets, cadmium coverages of 2.9 nm^{-2} and thus carboxylate coverages of 5.8 nm^{-2} are in principle possible. However, steric interactions between carboxylate ligands will prevent coverages from exceeding the density of crystalline alkane chains (4.9 chains/nm^2) on any given facet.[92] As a result, chain packing effects will prevent the coverage from reaching the upper limits defined by the underlying atomic surface density, and stable structures with a purely *n*-alkylcarboxylate ligand shell may never accommodate one cadmium for every surface selenium atom. Second, PLQY is known to drop during isolation of nanocrystals from crude synthesis mixtures, behavior that may derive from a change in the Cd^{2+} coverage.[52,63,93,94] Typically, an excess of unconverted $M(O_2CR)_2$ remains after synthesis, and its separation will reduce the solution concentration of $M(O_2CR)_2$ and can thereby change the coverage of weakly-bound metal cations.[50,52,95] A similar decrease in PLQY was observed in the present study where it is highest (~20%) prior to precipitation with methyl acetate and drops to ~10% as coverages of 3 carboxylates/nm^2 are reached. Both observations suggest that the ligand coverage obtained after isolation may be lower than that in the crude reaction mixtures produced by the nanocrystal synthesis.

Surface Cd^{2+} Coverage and Optical Properties

Changes to stoichiometry caused by isolation and exposure to Lewis bases helps explain the sensitivity of nanocrystal PLQY. Ligation is known to influence surface derived mid-gap electronic states, and thus it is not surprising that changes to the coverage of $Cd(O_2CR)_2$ influence the PLQY.[10,11,13,18,23,28,40,71,75,96,97] Previous studies have found that cadmium and zinc ions significantly improve PLQY and reduce photocharging when bound to nanocrystal surfaces. [21,27,41,53,68-76,98,99] Presumably these metal ions act as Z-type ligands, passivating mid gap states by binding surface Se sites and thereby preventing hole trapping.[10,25] With the exception of displacement reactions with primary *n*-alkylamines,

removing $Cd(O_2CR)_2$ in this study decreases PLQY with the greatest change being caused by dissolution of nanocrystals in neat TMEDA (PLQY < 0.1%). Plotting the PLQY versus cadmium coverage for isolated samples as well as samples measured *in situ* shows a strong super-linear correlation (Figure 4). PLQY is very sensitive to coverage above 2.5 carboxylates/nm^2, while samples with lower coverages are weakly photoluminescent. Samples exposed to primary amines, however, display significantly increased PLQY despite removing the greatest proportion of $Cd(O_2CR)_2$. The increase is related to the high coverage of amine ligands rather than an effect derived from the cadmium coverage;[18,36,38] the PLQY of isolated nanocrystals with low $Cd(O_2CR)_2$ coverage is greatest at higher amine concentrations. Thus PLQY is complex and depends on the presence of L-type donor ligands as well as Z-type accepter ligands in a manner that is very sensitive to coverages near saturation.

In addition to changing the PLQY, decreasing the $Cd(O_2CR)_2$ coverage to 0.6 carboxylates/nm^2 causes a slight red-shift (1 nm) in the wavelength of the lowest energy absorption, an effect that might be explained by a change in the local dielectric, or a change in the confining potential caused by the surface MX_2 layer (Figure 5).[28] While this red-shift could be attributed to nanocrystal aggregation, dynamic light scattering and transmission electron microscopy measurements show that the nanocrystals do not significantly aggregate upon reducing the carboxylate coverage to 0.6 carboxylates/nm^2 (Figure S15 and S16). As a result, the insensitivity of the lowest energy absorption is surprising given that ~85% of the surface $Cd(O_2CR)_2$ in this sample has been displaced, a ~10% reduction in the total number of cadmium ions in the nanocrystal. When calculating the volume change using the ionic radii of Cd^{2+} (109 pm) and Se^{28} (184 pm) and the void space of the unit cell,[100] this change in formula corresponds to a 3% decrease in volume and can be expected to produce a 4 nm blue-shift at this size.[101] Similar effects were observed in spectra of CdSe nanocrystals across a range of sizes from d = 3.3-3.7 nm where slightly larger red shifts are observed for smaller sizes (Figure S17). While the lowest energy absorption is not altered with a decrease in the cadmium ion coverage, higher energy transitions are significantly influenced. Removal of $Cd(O_2CR)_2$ from cadmium selenide or cadmium sulfide nanocrystals quenches the band-edge PLQY and decreases the apparent intensity of the $1S_e$-$2S_{3/2h}$ absorption (Figure 5). The narrow absorption features of cadmium sulfide nanocrystals clearly show the apparent intensity of the $1S_e$-$2S_{3/2h}$ absorption is reduced by broadening rather than a change in extinction (Figure S18).

The insensitivity of the first absorption energy to changes in the coverage of surface $Cd(O_2CR)_2$ is surprising and suggests that its 5*s* functions do not contribute significantly to the conduction nor valence band edges, and instead contribute to states within the bands. A related model was proposed to explain the influence of a Cd^{2+} layer on the energy difference between the first two electronic absorptions.[28] This study also focused on the reaction of nanocrystals with alkylamines, where changes in the intensity and energy of the second electronic absorption were observed, effects that may also stem from removal of $Cd(O_2CR)_2$ in their case. While others have noted a relationship between surface structure and the line-width of these higher energy transitions, the origin of these changes remains unclear.[31,84]

Changes to the nanocrystal absorbance and PLQY are reversed upon rebinding $Cd(O_2CR)_2$ at room temperature indicating that they are directly related to the coverage of Z-type ligands (Figure 5). While the absorbance and luminescence changes are only partially reversed upon stirring the nanocrystals with $Cd(O_2CR)_2$ at room temperature, they are completely reversed upon recovering the original surface ligand density at higher temperature (Figures 4 and 5C). Interestingly, similar changes are observed if nanocrystals with low carboxylate coverages are stirred with $CdCl_2$ rather than $Cd(O_2CR)_2$, corroborating a previous investigation of coordinatively unsaturated CdSe nanocrystals bound by tri-*n*-butylphosphine and cadmium chloride (Figure S19).[45] Together these observations support a general relationship between the coverage of cadmium ions and trap state passivation, as well as the optical spectrum of the nanocrystal.

Perspective

Several recent studies have investigated the influence of excess metal ions on mid- gap electronic states and doping. While we have shown that Cd^{2+} bound by X-type carboxylate ligands passivate surfaces, the oxidation state of the surface-bound metal ion will influence whether metal enrichment passivates charge trap states or contributes new mid-gap states. For example, the electron concentration in lead chalcogenide nanocrystal thin films can be increased by vapor depositing elemental lead (Pb^0).[57] Similarly, computational studies show that adsorption of Pb^0 atoms to nanocrystal surfaces adds filled electronic states within the band gap resulting in metallic-like behavior.[54] In the same study, these mid-gap states are removed when the surface lead atoms are converted to Pb^{2+} and balanced by X-type ligands. Thus the metal-rich stoichiometry of nanocrystals does not appear to create trap states when all ions are in their 2+ oxidation state.

Instead, cadmium and lead ions can passivate the nanocrystal by acting as electron-accepting Z-type ligands that lower the chalcogen-derived filled states of surface atoms. However, ideal passivation schemes should manage both filled and empty mid-gap states. Both chalcogen-derived filled states as well as metal-derived empty states can lead to mid-gap levels, and passivation of these empty levels by a high coverage of amine donors can also increase PLQY. The benefits of this approach have been demonstrated in PbS nanocrystal photovoltaic cells with record-breaking efficiencies.[4,44,53,102] Identifying surface passivating layers that bind both metal and chalcogen sites is therefore an important avenue of research.

A detailed understanding of metal ion binding affinities is needed to better understand and control these materials. While the metal-enrichment of cadmium and lead chalcogenide nanocrystals has been shown to increase with decreasing nanocrystal diameter according to the ratio of its surface area and volume,[34,49,50] we have shown that nanocrystals have a wide range of surface metal coverages. Thus the stoichiometry obtained is sensitive to the reagents and concentrations used to separate nanocrystals from unreacted $M(O_2CR)_2$ precursors. Nanocrystal stoichiometries are therefore not fixed for a given size and depend on the isolation method. In the present study, a particular stoichiometry was obtained using NMR spectroscopy as a guide to monitor bound and free $M(O_2CR)_2$ during precipitation. However, a wider range of stoichiometries can be obtained by altering the isolation method

including the solvents and concentrations used and the number of precipitation cycles as well as the binding affinity of the surface metal-surfactant layer.[16,17,52] In this sense, nanocrystals are not molecular; they do not have a single formula and nanocrystal purity is an indefinite concept. The method of synthesis can also influence the final stoichiometry.[50] For example, terminating a synthesis to obtain a desired size will influence the ratio of unconverted metal carboxylate and nanocrystals in the crude product.[63,103] As a consequence, the stoichiometry of the isolated product may not reflect the true size-dependence of the MX_2 binding, but instead the extent of precursor conversion and the effects of the isolation steps. Given the importance of stoichiometry to passivation, it is crucial that new synthetic methods precisely and systematically control stoichiometry in addition to optimizing a desired nanocrystal size and yield.

The effects of added Lewis bases on stoichiometry are also relevant to any post-synthesis modifications like exchange of native surfactant ligands. Many previous investigations of ligand exchange utilize photoluminescence intensity to monitor the extent of reaction unaware that stoichiometry may also change.[6,18,24,35,40,96,104] Some of these studies report conflicting results including the observation that primary amines can both increase and decrease PLQY. Similarly, PLQY has been used to measure the concentration dependence of ligand binding. From these data relative ligand binding constants were estimated, though only by assuming that coverage and PLQY are proportional. However, other studies point out that PLQY and ligation have a nonlinear relationship, where the binding of even a single octanethiol molecule can quench the luminescence by at least 50%.[23] Our direct correlation of PLQY and $Cd(O_2CR)_2$ surface coverage demonstrates that there is a threshold of 2 carboxylates/nm^2 below which the PLQY is ≤ 1% and above which PLQY rapidly increases. Hence, PLQY and ligation are not simply related, both because of their nonlinear interdependence but also because displacement of $Cd(O_2CR)_2$ can occur concurrently with amine binding.

Stoichiometry is also important to the optoelectronic properties of nanocrystal thin films and methods must be designed that exchange X-type ligands while maintaining stoichiometry during film deposition. Traditional approaches to fabricate conductive nanocrystal films displace native surfactant ligands with pyridine,[4,91,105-110] primary alkylamines,[15,73,111-116] hydrazine[73,84,106,108,116-126] and alkane diamines,[3,4,73,84,108,113,114,118,127-133] and are therefore likely to significantly reduce the metal-enrichment. Chelating alkane diamines have been used to displace native ligands and link nanocrystals, resulting in films where the inter-nanocrystal spacing depends on the diamine chain length.[73,84,108,113,114,128-130,132,133] Our results show the $M(O_2CR)_2$ displacement efficiency depends on the diamine chain length because chelation stabilizes the displaced metal complex. The inter-nanocrystal distance measured in those studies may result, at least in part, from the relative displacement potency of the diamine. Indeed some of these studies report changes to the absorption and photoluminescence spectra, such as quenching of the PLQY and changes to the $1S_e$-$2S_{3/2h}$ absorption, similar to those described above.[31,84,114]

Recent approaches to thin film fabrication that utilize thiocyanate, sulfide, halide, and metal-chalcogenide salts can, in principle, exchange X-type ligands without altering stoichiometry.[4,41,44,53,75,102,134-136] However, the affinity of the new surface MX_2

complexes for the nanocrystal likely depends on the nature of both the cation and the anion, and therefore the resulting MX_2 complex may be more weakly bound than the starting metal-surfactant layer. In the case of chloride exchange, cadmium chloride appears to be a weaker Z-type ligand for the nanocrystal core than cadmium carboxylate,[45] perhaps because the carboxylate binds in a bidentate fashion.[137] Identifying ligand exchange methods that optimize inter-nanocrystal electronic coupling while maintaining a high coverage of MX_2 should produce conductive nanocrystal films with minimal trap state densities.[44]

Conclusion

The lability of the Z-type MX_2 layer is a key aspect of nanocrystal reactivity that explains the mechanisms of previously reported ligand exchange reactions. Various neutral ligands drive the displacement of $Cd(O_2CR)_2$ from CdSe nanocrystals in a manner that depends sensitively on the ligand concentration, steric profile, chelation, and hard/soft match with the cadmium center. Mixtures of chelating alkanediamines and primary alkylamines displace > 90% of the surface-bound $Cd(O_2CR)_2$ resulting in alkylamine-bound nanocrystals with carboxylate coverages as low as 0.3 ± 0.1 nm^{-2}. This type of reactivity appears to be general for zincblende CdSe and CdS as well as rock salt PbS and PbSe nanocrystals. Changes to the nanocrystal stoichiometry strongly influence the optical properties of these materials. In particular, a decrease in the surface-bound $Cd(O_2CR)_2$ is shown to greatly reduce the apparent intensity of the $1S_e$-$2S_{h3/2}$ transition without significantly influencing the lowest energy absorption. The PLQY is also quenched by decreasing the carboxylate coverage, particularly when coverages below 2 carboxylates nm^{-2} are reached. This effect is likely derived from the interaction of surface cadmium ions with mid-gap chalcogen derived states. The displacement reactivity proved rapid and reversible, as did the corresponding changes to the optical properties, behavior that helps explain the sensitivity of nanocrystal luminescence.

Cadmium and lead chalcogenide nanocrystals have chemical formulas that are dynamic at room temperature and depend on the solution composition. Thus, any definition of their purity is arbitrary. However, it is of utmost importance that the solutions in which the nanocrystals are handled, and in particular the extent to which Z-type and L-type ligands are separated during isolation, is carefully managed. Without controlling their chemical formulas, understanding the relationship between nanocrystal properties and structure will be difficult. This underscores the need for improved syntheses, isolation procedures, and ligand exchange methods that manage stoichiometry.

Experimental Section

General Methods

Cadmium nitrate tetra-aquo (99%), lead (II) oxide (reagent grade) sodium hydroxide, myristic acid (99%), selenium dioxide (99.8%), anhydrous oleic acid (99%), 1-tetradecanol (95%), eladic acid (99%), methanol (99.8%), hexamethyldisilathiane (synthesis grade), and 1-octadecene (90%) were purchased from Sigma Aldrich and used as received. Ferrocene (98%) was purchased from Sigma Aldrich and purified by sublimation before use. d_6-Benzene (99.6%), anhydrous acetonitrile (99.5%), and anhydrous methyl acetate (99.5%)

were purchased from Sigma Aldrich, shaken with activated alumina, filtered, and stored over 4 Å molecular sieves in an inert atmosphere glove box at least 24 hours prior to use. Pentane, tetrahydrofuran, and toluene were dried over alumina columns, shaken with activated alumina, filtered and stored over 4 Å molecular sieves in an inert atmosphere glove box at least 24 hours prior to use. Diphenylphosphine (99%), N,N,'N,'N-tetramethylethylene-1,2-diamine (TMEDA) (98%), tri-*n*-octylphosphine (97%) and tri-*n*-butylphosphine (99%) were purchased from Strem and used without further purification. $CdMe_2$ was purchased from Strem and vacuum distilled prior to use. CAUTION: Dimethylcadmium is extremely toxic and because of its volatility and air-sensitivity should only be handled by a highly trained and skilled scientist. N,N-dimethylbutylamine (98%), N,N,N',N'-tetramethyl-1,4-butane diamine (97%), 1-nonanyl nitrile (98%), tri-*n*-butylamine (99%), *n*-octylamine (99%), and pyridine (99.5%) were purchased from Sigma Aldrich and dried over CaH_2, distilled, and stored in a nitrogen glove box. Cadmium tetradecanoate was synthesized from cadmium nitrate and tetradecanoic acid on 25 mmol scale following a procedure reported previously.[93] Cadmium oleate and cadmium eliadate were synthesized by adding the appropriate carboxylic acid in a 1:2 ratio to dimethyl cadmium dissolved in pentane. The resulting white powder was filtered and dried under vacuum.

All manipulations were performed under air-free conditions unless otherwise indicated using standard Schlenk techniques or within a nitrogen atmosphere glove box. NMR spectra were recorded on Bruker Avance III 500 MHz instruments. ^{1}H NMR spectra were acquired with sufficient relaxation delay to allow complete relaxation between pulses (30 seconds). UV-Visible data was obtained using a Perkin Elmer Lambda 650 or 950 spectrophotometers equipped with deuterium and tungsten halogen lamps. Photoluminescence spectra and quantum yield were measured using a FluoroMax-4 equipped with an Integrating Sphere from Horiba Scientific. FT-IR spectra were obtained on a Thermo Scientific Nicolet 6700 spectrometer equipped with a liquid N_2 cooled MCT-A detector. RBS measurements were conducted at the University of Western Ontario in the Interface Science Western facility.

CdSe nanocrystals

Carboxylate terminated zincblende CdSe nanocrystals were synthesized using a previously reported procedure.[93] Typical reactions were run using 10 mmol of cadmium tetradecanoate and a Cd:Se ratio of 1. Isolated nanocrystals were dissolved in d_6-benzene and the vinyl region of the ^{1}H NMR spectrum was used to detect unbound ligands. Samples without signals from free oleyl chains were used to make d_6-benzene stock solutions for ligand exchange studies. Typical stock solutions ($[^-O_2CR]$ = ~ 200 mM; [nanocrystal] = ~ 2 mM) were diluted for NMR spectroscopy ($[^-O_2CR]$ = ~ 20 mM) and for UV-visible absorption spectroscopy and PLQY measurements ($[^-O_2CR]$ = ~ 0.2 μM).

CdS nanocrystals

Tetradecanoate terminated zincblende CdS nanocrystals were synthesized and isolated at 2× the concentration and 5× the volume reported previously.[63] It is worth noting that the isolation procedure involves precipitating the nanocrystals from a TMEDA/toluene solution, rather than methyl acetate. Isolated nanocrystals were dissolved in d_6-benzene and the methyl region of the ^{1}H NMR spectrum was used to confirm that no free ligands were

present. Typical stock solutions used for NMR spectroscopy ([$^{-}O_2CR$] = ~ 10 mM; [nanocrystal] = ~ 0.3 mM) were diluted for UV-visible absorption spectroscopy and PLQY measurements ([$^{-}O_2CR$] = ~ 0.3 μM).

PbS nanocrystals

PbS nanocrystals were synthesized using a previously reported procedure.[138] Typical reactions were run at 50 mL scale using of lead (II) oxide (0.12 molar), oleic acid (1.2 molar), and Pb:S ratio of 2:1. Isolated nanocrystals were dissolved in d_6-benzene and the vinyl region of the ^{1}H NMR spectrum was used to analyze the sample for free ligands. Samples without signals from free oleyl chains were used to make d_6-benzene stock solutions for ligand exchange studies. Typical stocks used for NMR spectroscopy ([$^{-}O_2CR$] = ~ 50 mM; [nanocrystal] = ~ 0.4 mM) were diluted for UV-Vis-NIR measurements ([nanocrystal] = ~ 0.4 μM).

PbSe nanocrystals

PbSe nanocrystals were synthesized using a previously reported procedure.[139] Typical reactions were run at 50 ml scale using lead (II) oxide (0.1 molar), oleic acid (0.3 molar), and a Pb:Se:diphenylphosphine ratio of 1:2:0.2. Isolated nanocrystals were dissolved in d_6-benzene and the vinyl region of the ^{1}H NMR spectrum used to analyze the sample for free ligands. Samples without signals from free oleyl chains were used to make d_6-benzene stock solutions for ligand exchange studies. Typical stocks used for NMR spectroscopy ([$^{-}O_2CR$] = ~ 20 mM; [nanocrystal] = ~ 0.1 mM) were diluted for UV-Vis-NIR measurements ([nanocrystal] = ~ 0.1 μM).

Measurement of the ligand and ME concentration

The concentrations of nanocrystals and carboxylate or amine ligands in d_6-benzene stock solutions were determined using a combination of NMR and UV-Visible absorption spectroscopies. Ferrocene dissolved in d_6-benzene (10 μl, 0.05 M) was added to a known volume of the nanocrystal stock solution and used as an internal standard. The concentration of ligands was determined relative to the internal ferrocene standard by integrating the ligand methyl and ferrocene resonances and normalizing for the number of hydrogens respectively (3:10). Nanocrystals with *n*-octylamine ligands were precipitated from neat *n*-octylamine using methylacetate, isolated by centrifugation and twice reprecipitated from pentane solution with methylacetate to ensure that the remaining amine is all derived from surface bound ligands, rather than adventitious amine. [45,140] The molar concentration of CdSe, CdS, PbS, and PbSe nanocrystals in these stock solutions was determined by diluting 10-30 μl to a known volume with toluene and measuring the absorbance at λ = 350 nm for CdSe and CdS nanocrystals and at λ = 400 nm for PbS and PbSe nanocrystals. At these wavelengths the extinction coefficient is independent of size.[141,142,47,143]

Calculation of ligand per particle and ME units per ligand ratios

The wavelength of the lowest absorption maximum was used to determine the average nanocrystal diameter[144,142] The diameter of PbS and PbSe nanocrystals were determined from the wavelength of the lowest energy absorption feature according to Hens.[47,143] From

this diameter the number of ME (M = Cd, Pb; E = Se, S) units per nanocrystal were calculated by assuming a spherical shape and the molar volume of the bulk. The concentration of nanocrystals, the ratio of ligands per nanocrystal and the ligand surface density assuming a spherical shape were calculated from the number of ME units per nanocrystal, the molar concentration of ME, and ligands in the stock solution.

Photoluminescence quantum yield measurements

PLQY were measured using a Fluoromax-4 Fluorometer equipped with an integrating sphere. Samples were diluted to concentrations below 0.1 absorbance units at the 1Se-1Sh1/2 to minimize reabsorption. Data are not corrected for reabsorption and are therefore an underestimate. A blank sample of toluene was used to adjust the excitation and emission slits to avoid saturating the detector, and photoluminescence spectra, including the excitation wavelengths, were recorded for both the toluene blank and the nanocrystal solution. The number of photons absorbed by the sample was determined by measuring the difference between the blank and the sample at the excitation wavelength, and the photoluminescence spectrum of the nanocrystal solution was integrated from 500-650 nm to determine the photons emitted. PLQY was calculated from the ratio of photons emitted and photons absorbed. The validity of this approach was evaluated using freshly prepared solutions of Coumarin-153 in ethanol (PLQY = 53%).[145]

Isolation of cadmium carboxylate removed from CdSe nanocrystals with Bu_3P or TMEDA

CdSe nanocrystals (4 g) were dissolved in a d_6-benzene solution of Bu_3P or TMEDA (8 ml, 0.5 M) and stirred for 3 hours. The solution was diluted to a total volume of 30 ml, and methylacetate was added to a total volume to 90 ml causing precipitation of the nanocrystals. After separation of the nanocrystals by centrifugation (7000 RPM for 5 minutes), the clear, colorless supernatant was decanted and the nanocrystals dissolved in 15 ml of toluene and precipitated a second time with methyl acetate. The nanocrystals were separated by centrifugation and the clear, colorless supernatant decanted. This process was repeated a third time, after which the nanocrystals were discarded, and the combined supernatants dried under vacuum. A clear oil remained which had faint but perceptible pink hue, that was dissolved in toluene and diluted with methyl acetate to precipitate any remaining nanocrystals, which were separated by centrifugation. The volatiles were removed under vacuum and the residue again dissolved in toluene, diluted with methyl acetate and centrifuged to remove any remaining nanocrystals. The resulting clear solution was distilled to dryness under vacuum and dried for 3 hours, resulting in a clear, pale yellow oil that was analyzed with NMR, infrared absorption, and x-ray photoelectron spectroscopies. **Removal with Bu_3P**: ^{1}H NMR (C_6D_6, 500 MHz): δ = 0.93 (m, 15H, $-CH_3$), 1.1-1.6 (b, 62H, $-CH_2$, $-CH_2P$), 1.84 (m, 4H, $\beta-CH_2$), 2.08 (m, 8H, $-C{=}CCH_2$), 2.52 (t, 4H, $\alpha-CH_2$), 5.48 (m, 4H, −CH=CH), 13.7 (b, −COOH). $^{31}P\{^1H\}$ NMR (C_6D_6, 202.4 MHz): δ = −16.7 (b). FT-IR (Diamond ATR): ν = 1384 cm^{-1} (*s* CO_2 *assym*), 1564 cm^{-1} (*s* CO_2 *sym*), 1730 cm^{-1} (*w* COOH), 2925 cm^{-1} (*s* C-H). **Removal with TMEDA**: ^{1}H NMR (C_6D_6, 500 MHz): δ = 0.91 (t, 6H, $-CH_3$), 1.2-1.6 (b, 44H, $-CH_2$), 1.84 (m, 4H, β-CH_2), 1.94 (s, 4H, - NCH_2), 2.09 (m, 8H, $-C{=}CCH_2$), 2.24 (s, 12H, $-N(CH_3)_2$), 2.52 (t, 4H, α-CH_2), 5.49 (m, 4H, 8 CH=CH), 9.3 (b, -NH). FT-IR (Diamond ATR): ν = 1382 cm^{-1} (*s* CO_2 *assym*), 1560 cm^{-1} (*s* CO_2 *sym*), 1720 cm^{-1} (*w* COOH), 2920 cm^{-1} (*s* C-H).

Isolation of cadmium carboxylate removed from CdSe nanocrystals with methanol

CdSe nanocrystals (1.86 g) were dissolved in toluene (10 ml) and removed from the glove box in a centrifuge tube. In air, methanol was added to a total volume to 50 ml causing precipitation of the nanocrystals. After separation of the nanocrystals by centrifugation (7000 RPM for 5 minutes), the clear, colorless supernatant was decanted and saved. The nanocrystals were then dissolved in 10 ml of toluene, precipitated a second time with methanol, separated by centrifugation, and the clear, colorless supernatant decanted and saved. This process was repeated three additional times, after which the nanocrystals were discarded, and the combined supernatants distilled to dryness under vacuum. A clear faintly pink oil remains that was dissolved in toluene and diluted with methanol to precipitate any remaining nanocrystals. which were removed by centrifugation. This process was repeated once and the final clear supernatant was distilled to dryness under vacuum, resulting in a clear, pale yellow oil that was analyzed with NMR and infrared absorption spectroscopies. ^{1}H NMR (C_6D_6, 500 MHz): δ = 0.95 (m, 6H, −CH_3), 1.181.5 (b, 44H, −CH_2), 1.84 (m, 4H, β-CH_2), 2.1 (m, 8H, −C=CCH_2), 2.52 (t, 4H, α-CH_2), 5.49 (m, 4H, −CH=CH) FT-IR (Diamond ATR): ν = 1383 cm^{-1} (*s* CO_2 *assym*), 1564 cm^{-1} (*s* CO_2 *sym*), 2925 cm^{-1} (*s* C-H) 3200 cm^{-1} (*b* O-H).

Isolation of lead carboxylate removed from PbS nanocrystals with TMEDA

PbS nanocrystals (0.5 g) were dissolved in d_6-benzene (2 mL) and TMEDA (3 mL) was added. After stirring for 10 minutes, acetonitrile (5 mL) was added and the nanocrystals separated by centrifugation. The clear supernatant was collected and dried under vacuum for 5 hours. d_6-benzene (0.6 ml) was added to dissolve the residue and the solution was analyzed with ^{1}H NMR spectroscopy. Infrared absorption spectroscopy was performed using diffuse reflectance geometry as a mixture with KBr. Energy dispersive X-ray spectroscopy was conducted on a film drop-cast on a highly ordered pyrolitic graphite substrate using a Cold Field Emission Hitachi 4700 Scanning Electron Microscope. ^{1}H NMR (C_6D_6, 500 MHz): δ = 0.91 (t, 6H, −CH_3), 1.281.6 (b, 44H, −CH_2), 1.84 (m, 4H, β-CH_2), 1.94 (s, 4H, −NCH_2), 2.09 (m, 8H, −C=CCH_2), 2.24 (s, 12H, −$N(CH_3)_2$), 2.52 (t, 4H, α-CH_2), 5.49 (m, 4H, −CH=CH), 9.3 (b, −NH). FT-IR (Diamond ATR): ν = 1384 cm^{-1} (*s* CO_2 *assym*), 1560 cm^{-1} (*s* CO_2 *sym*), 1720 cm^{-1} (*w* COOH), 2920 cm^{-1} (*s* C-H).

Correlation between PLQY and percent $Cd(O_2CR)_2$ displacement measurements

In a J-Young NMR tube, a 0.02 M solution of a desired ligand was prepared by adding the ligand (10 μl of a 1.1 M d_6-benzene stock solution) to a 590 μl stock solution of nanocrystals in d_6-benzene (0.02 M in - O_2CR). For higher concentrations (0.2 M and 2.0M), a second and third addition of ligand were added (1.1 × 10^{-4} mol and 1.1 × 10^{-3} mol respectively). ^{1}H NMR spectra were acquired within 10 minutes after ligand addition. The among of ligand displaced was determined by integrating the sharp resonance of free oleyl chains as a percentage of total vinyl region. Separate stock solutions of nanocrystals (2.4 × 10^{-5} M in ^-O_2CR) and 0.02 M, 0.2 M, and 2.0 M in displacement ligand were prepared in quartz cuvettes under nitrogen for PLQY measurements.

Error Analysis

Assuming a precision of a Cd-Se bond distance (~ 0.2 nm) in the diameter determination leads to the errors shown for the number of ME units in each nanocrystal. When calculating the number of ligands per nanocrystal, we estimate 10% error in the integration of the broad NMR signals and 5% error in the concentration of dilutions used to measure UV-Vis absorption. Volume additivity was assumed when calculating concentrations. RBS has a precision of 5%.

Isolation of CdSe nanocrystals with minimal $Cd(O_2CR)_2$ coverage

TMEDA (2 ml) was added to a stock solution of CdSe nanocrystals (2 ml, $[^{-}O_2CR] = 0.2$ M) and stirred for 1 hour. Nanocrystals were isolated by precipitation using methyl acetate and centrifugation. The red precipitate was dissolved in 5 ml of toluene and isolated by precipitation and centrifugation an additional 2 times. After the final centrifugation the nanocrystals were dissolved in pentane, dried under vacuum, and characterized by NMR and UV-visible absorption spectroscopies. Dynamic light scattering and transmission electron microscopy measurements show that nanocrystals with this ligand coverage are unaggreated (see supporting information).

Rebinding of $Cd(O_2CR)_2$

For CdSe: In a three-neck round-bottom flask equipped with a thermocouple adapter, reflux condenser, and septum, 100 mg of cadmium elaidate, 25 mg of oleic acid, and 5 ml of a 0.08 M (in $^{-}O_2CR$) solution of CdSe nanocrystals in 18octadecene were degassed and then heated to 240 °C under argon for 1 hour. The solution was then transferred via cannula to a Teflon stoppered Schlenk flask and transported to a glove box. Nanocrystals were isolated using three cycles of dissolution in tetrahydrofuran and precipitation with methyl acetate. Tetrahydrofuran was necessary to separate the polymeric cadmium carboxylate. The isolated nanocrystals were dried under vacuum and dissolved in $d_6$8benzene for NMR and UV-vis analysis. *For CdS*: In a nitrogen-filled glove box, a 0.05 mM (in nanocrystals) solution of TMEDA-treated CdS nanocrystals (see CdS synthesis above) in C_6D_6 (2 mL) was combined with THF (5 mL) in a vial charged with a stir bar. Cadmium oleate powder (300 mg; 390 mmol) was added to this solution, which was left to stir for >3 hours. Nanocrystals were isolated using one cycle of dissolution in tetrahydrofuran and precipitation with methyl acetate, followed by two cycles of dissolution in pentane and precipitation with methyl acetate. The isolated nanocrystals were dried under vacuum and dissolved in d_6-benzene for NMR and UV-vis analysis. This sample was used for Figure S5.

Supplementary Material

Refer to Web version on PubMed Central for supplementary material.

ACKNOWLEDGMENT

This work was funded by the Department of Energy under Grant No. DE-SC0006410. NCA acknowledges support from the National Science Foundation under Grant No. DGE07807425. The authors also thank Columbia University for support. We thank Prof. Lyudmila Goncharova from the Interface Science Western Research at the University of Western Ontario for Rutherford backscattering spectrometry analysis. We acknowledge Zachariah M. Norman for useful discussions and assistance with dynamic light scattering measurements. Alexander N. Beecher

and William Rice are acknowledged for assistance with TEM, which was conducted at the New York Structural Biology Center constructed with support from Research Facilities Improvement Program Grant number C06 RR0175288018CEM from the National Center for Research Resources, National Institutes of Health.

REFERENCES

1. Kamat PV. J. Phys. Chem. C. 2008; 112:18737–18753.
2. Kramer IJ, Sargent EH. ACS Nano. 2011; 5:8506–8514. [PubMed: 21967723]
3. Talapin DV, Lee JS, Kovalenko MV, Shevchenko EV. Chem. Rev. 2010; 110:389–458. [PubMed: 19958036]
4. Tang JA, Sargent EH. Adv. Mater. 2011; 23:12–29. [PubMed: 20842658]
5. Wuister SF, Swart I, Driel FV, Hickey SG, Donega CDM. Nano Lett. 2003; 3:503–507.
6. Galian RE, Scaiano JC. Photochem. Photobiol. Sci. 2009; 8:70874.
7. Wang Y, Hu R, Lin G, Roy I, Yong K-T. ACS Appl. Mater. Interfaces. 2013; 5:2786–2799. [PubMed: 23394295]
8. Ma G. ACS Appl. Mater. Interfaces. 2013; 5:2835–2844. [PubMed: 23448359]
9. Argeri M, Fraccarollo A, Grassi F, Marchese L, Cossi M. J. Phys. Chem. C. 2011; 115:11382–11389.
10. Bawendi MG, Carroll PJ, Wilson WL, Brus LE. J. Chem. Phys. 1992; 96:946–954.
11. Bryant GW, Jaskolski W. J. Phys. Chem. B. 2005; 109:19650–19656. [PubMed: 16853541]
12. Cossairt BM, Juhas P, Billinge S, Owen JS. J. Phys. Chem. Lett. 2011; 2:3075–3080. [PubMed: 22229074]
13. Fischer SA, Crotty AM, Kilina SV, Ivanov SA, Tretiak S. Nanoscale. 2012; 4:904–914. [PubMed: 22170563]
14. Green M. J. Mater. Chem. 2010; 20:5797–5809.
15. Guyot-Sionnest P, Wehrenberg B, Yu D. J. Chem. Phys. 2005; 123:074709. [PubMed: 16229612]
16. Hartmann L, Kumar A, Welker M, Fiore A, Julien-Rabant C, Gromova M, Bardet M, Reiss P, Baxter PNW, Chandezon F, Pansu RB. ACS Nano. 2012; 6:9033–9041. [PubMed: 23009087]
17. Hassinen A, Moreels I, De Nolf K, Smet PF, Martins JC, Hens Z. J. Am. Chem. Soc. 2012; 134:20705–20712. [PubMed: 23190352]
18. Kalyuzhny G, Murray RW. J. Phys. Chem. B. 2005; 109:7012–7021. [PubMed: 16851797]
19. Kuno M, Lee JK, Dabbousi BO, Mikulec FV, Bawendi MG. J. Chem. Phys. 1997; 106:9869–9882.
20. Landes C, Burda C, Braun M, El-Sayed MA. J. Phys. Chem. B. 2001; 105:2981–2986.
21. Liu H, Guyot-Sionnest P. J. Phys. Chem. C. 2010; 114:14860–14863.
22. Moreels I, Justo Y, De Geyter B, Haustraete K, Martins JC, Hens Z. ACS Nano. 2011; 5:2004–2012. [PubMed: 21355621]
23. Munro AM, Ginger DS. Nano Lett. 2008; 8:2585–2590. [PubMed: 18578549]
24. Munro AM, Jen-La Plante I, Ng MS, Ginger DS. J. Phys. Chem. C. 2007; 111:6220–6227.
25. Nirmal M, Murray CB, Norris DJ, Bawendi MG. Z. Phys. D-Atoms Mol. Clusters. 1993; 26:361–363.
26. Talapin DV, Rogach AL, Kornowski A, Haase M, Weller H. Nano Lett. 2001; 1:207–211.
27. Spanhel L, Haase M, Weller H, Henglein A. J. Am. Chem. Soc. 1987; 109:5649–5655.
28. Chen O, Yang YA, Wang T, Wu HM, Niu CG, Yang JH, Cao YC. J. Am. Chem. Soc. 2011; 133:17504–17512. [PubMed: 21954890]
29. Dannhauser T, Oneil M, Johansson K, Whitten D, McLendon G. J. Phys. Chem. 1986; 90:6074–6076.
30. Donakowski MD, Godbe JM, Sknepnek R, Knowles KE, de la Cruz MO, Weiss EA. J. Phys. Chem. C. 2010; 114:22526–22534.
31. Dzhagan VM, Lokteva I, Himcinschi C, Kolny-Olesiak J, Valakh MY, Schulze S, Zahn DRT. J. Appl. Phys. 2011; 109:084334.
32. Fritzinger B, Capek RK, Lambert K, Martins JC, Hens Z. J. Am. Chem. Soc. 2010; 132:10195–10201. [PubMed: 20608680]

33. Gomes R, Hassinen A, Szczygiel A, Zhao Q, Vantomme A, Martins JC, Hens Z. J. Phys. Chem. Lett. 2011; 2:145–152.
34. Hughes BK, Ruddy DA, Blackburn JL, Smith DK, Bergren MR, Nozik AJ, Johnson JC, Beard MC. ACS Nano. 2012; 6:5498–5506. [PubMed: 22571723]
35. Ji XH, Copenhaver D, Sichmeller C, Peng XG. J. Am. Chem. Soc. 2008; 130:5726–5735. [PubMed: 18396878]
36. Kim W, Lim SJ, Jung S, Shin SK. J. Phys. Chem. C. 2010; 114:1539–1546.
37. Koole R, Schapotschnikow P, Donegá CDM, Vlugt TJH, Meijerink A. ACS Nano. 2008; 2:1703–1714. [PubMed: 19206375]
38. Li RF, Lee J, Yang B, Aindow M, Papadimitrakopoulos F. Abstr. Pap. Am. Chem. Soc. 2005; 230:U1163–U1164.
39. Luo X, Liu P, Tam N, Truong N, Farva U, Park C. J. Phys. Chem. C. 2011; 115:20817–20823.
40. von Holt B, Kudera S, Weiss A, Schrader TE, Manna L, Parak WJ, Braun M. J. Mat. Chem. 2008; 18:2728–2732.
41. Ip AH, Thon SM, Hoogland S, Voznyy O, Zhitomirsky D, Debnath R, Levina L, Rollny LR, Carey GH, Fischer A, Kemp KW, Kramer IJ, Ning Z, Labelle AJ, Chou KW, Amassian A, Sargent EH. Nat. Nano. 2012; 7:577–582.
42. Morris-Cohen AJ, Malicki M, Peterson MD, Slavin JWJ, Weiss EA. Chem. Mat. 2013; 25:1155–1165.
43. Owen JS, Park J, Trudeau P-E, Alivisatos a. P. J. Am. Chem. Soc. 2008; 130:12279–12281. [PubMed: 18722426]
44. Voznyy O, Zhitomirsky D, Stadler P, Ning Z, Hoogland S, Sargent EH. ACS Nano. 2012; 6:8448–8455. [PubMed: 22928602]
45. Anderson NC, Owen JS. Chem. Mat. 2013; 25:69–76.
46. Depictions of nanocrystals in Schemes 1, 2, and 3 provide graphical depiction of chemical formula and do not address underlying structure of the nanocrystal core, nor do they imply surface ligand confirmations. For example, computational studies of complete carboxylate terminated nanocrystals indicate that each carboxylate ion binds separate metal ion sites in a bidendate fashion. See Ref 11, 44, and 112.
47. Moreels I, Fritzinger B, Martins JC, Hens Z. J. Am. Chem. Soc. 2008; 130:15081–15086. [PubMed: 18928251]
48. Caldwell MA, Albers AE, Levy SC, Pick TE, Cohen BE, Helms BA, Milliron D. J. Chem. Commun. 2011; 47:556–558.
49. Dai Q, Wang Y, Li X, Zhang Y, Pellegrino DJ, Zhao M, Zou B, Seo J, Wang Y, Yu WW. ACS Nano. 2009; 3:1518–1524. [PubMed: 19435305]
50. Morris-cohen AJ, Frederick MT, Lilly GD, Mcarthur EA, Weiss EA. J. Phys. Chem. Lett. 2010; 1:1078–1081.
51. Smith DK, Luther JM, Semonin OE, Nozik AJ, Beard MC. ACS Nano. 2011; 5:183–190. [PubMed: 21141910]
52. Morris-Cohen AJ, Donakowski MD, Knowles KE, Weiss EA. J. Phys. Chem. C. 2010; 114:897–906.
53. Tang J, Kemp KW, Hoogland S, Jeong KS, Liu H, Levina L, Furukawa M, Wang X, Debnath R, Cha D, Chou KW, Fischer A, Amassian A, Asbury JB, Sargent EH. Nature Materials. 2011; 10:765–771.
54. Kim D, Kim D-H, Lee J-H, Grossman JC. Phys. Rev. Lett. 2013; 110:196802. [PubMed: 23705733]
55. Luther JM, Pietryga JM. ACS Nano. 2013; 7:1845–1849. [PubMed: 23527749]
56. Kim, DK.; Fafarman, AT.; Diroll, BT.; Chan, SH.; Gordon, TR.; Murray, CB.; Kagan, CR. ACS Nano. ASAP; 2013. DOI: 10.1021/nn403132x
57. Oh SJ, Berry NE, Choi J-H, Gaulding EA, Paik T, Hong S-H, Murray CB, Kagan CR. ACS Nano. 2013; 7:2413–2421. [PubMed: 23368728]
58. Jasieniak J, Mulvaney P. J. Am. Chem. Soc. 2007; 129:2841–2848. [PubMed: 17309253]
59. Soni U, Sapra S. J. Phys. Chem. C. 2010; 114:22514–22518.

60. Wei HH-Y, Evans CM, Swartz BD, Neukirch AJ, Young J, Prezhdo OV, Krauss TD. Nano Lett. 2012; 12:4465–4471. [PubMed: 22924603]
61. Zhang HT, Hu B, Sun LF, Hovden R, Wise FW, Muller DA, Robinson RD. Nano Lett. 2011; 11:5356–5361. [PubMed: 22011091]
62. Donega CD, Hickey SG, Wuister SF, Vanmaekelbergh D, Meijerink A. J. Phys. Chem. B. 2003; 107:489–496.
63. Hendricks MP, Cossairt BM, Owen JS. ACS Nano. 2012; 6:10054–10062. [PubMed: 23043371]
64. Omogo B, Aldana JF, Heyes CD. J. Phys. Chem. C. 2013; 117:2317–2327.
65. Ouyang JY, Kuijper J, Brot S, Kingston D, Wu XH, Leek DM, Hu MZ, Ripmeester JA, Yu K. J. Phys. Chem. C. 2009; 113:7579–7593.
66. Qu LH, Peng XG. J. Am. Chem. Soc. 2002; 124:2049–2055. [PubMed: 11866620]
67. Sharma SN, Pillai ZS, Kamat PV. J. Phys. Chem. B. 2003; 107:10088–10093.
68. Casavola M, van Huis MA, Bals S, Lambert K, Hens Z, Vanmaekelbergh D. Chem. Mat. 2012; 24:294–302.
69. Kovalenko MV, Talapin DV, Loi MA, Cordella F, Hesser G, Bodnarchuk MI, Heiss W. Angew. Chem. Int. Edit. 2008; 47:3029–3033.
70. Pietryga JM, Werder DJ, Williams DJ, Casson JL, Schaller RD, Klimov VI, Hollingsworth JA. J. Am. Chem. Soc. 2008; 130:4879–4885. [PubMed: 18341344]
71. Abel KA, FitzGerald PA, Wang T-Y, Regier TZ, Raudsepp M, Ringer SP, Warr GG, van Veggel FCJM. J. Phys. Chem. C. 2012; 116:3968–3978.
72. Liu D, Snee PT. ACS Nano. 2011; 5:546–550. [PubMed: 21141814]
73. Beard MC, Midgett AG, Law M, Semonin OE, Ellingson RJ, Nozik AJ. Nano Lett. 2009; 9:836–845. [PubMed: 19170560]
74. Midgett AG, Hillhouse HW, Hughes BK, Nozik AJ, Beard MC. J. Phys. Chem. C. 2010; 114:17486–17500.
75. Nag A, Chung DS, Dolzhnikov DS, Dimitrijevic NM, Chattopadhyay S, Shibata T, Talapin DV. J. Am. Chem. Soc. 2012; 134:13604–13615. [PubMed: 22812398]
76. Kovalenko MV, Schaller RD, Jarzab D, Loi MA, Talapin DV. J. Am. Chem. Soc. 2012; 134:2457–2460. [PubMed: 22239647]
77. Becerra LR, Murray CB, Griffin RG, Bawendi MG. J. Chem. Phys. 1994; 100:3297–3300.
78. Wang F, Tang R, Buhro WE. Nano Lett. 2008; 8:3521–3524. [PubMed: 18754691]
79. Wang F, Tang R, Kao JL-F, Dingman SD, Buhro WE. J. Am. Chem. Soc. 2009; 131:4983–4994. [PubMed: 19296595]
80. Green MLH. J. Organomet. Chem. 1995; 500:127–148.
81. Capek RK, Moreels I, Lambert K, De Muynck D, Zhao Q, Vantomme A, Vanhaecke F, Hens Z. J. Phys. Chem. C. 2010; 114:6371–6376.
82. Hens Z, Martins JC. Chem. Mater. 2013; 25:1211–1221.
83. Malicki M, Knowles KE, Weiss EA. Chem. Commun. 2013; 49:4400–4402.
84. Vercelli B, Zotti G, Berlin A. J. Phys. Chem. C. 2011; 115:4476–4482.
85. Knittel, F.; Gravel, E.; Cassette, E.; Pons, T.; Pillon, F.; Dubertret, B.; Doris, E. Nano Lett. ASAP; 2013. DOI: 10.1021/nl402192d
86. Dai Q, Zhang Y, Wang Y, Wang Y, Zou B, Yu WW, Hu MZ. J. Phys. Chem. C. 2010; 114:16160–16167.
87. Murray CB, Norris DJ, Bawendi MG. J. Am. Chem. Soc. 1993; 115:8706–8715.
88. The slight red8shift (~1 nm) in the absorption spectrum and the absence of Se in the isolated supernatant show that the displacement reaction reported herein is distinct from previous observations of “etching”. These studies report blue shifts of the first exciton peak as both metal and chalcogenide ions are lost and the nanocrystals decrease in diameter.
89. Schwarzenbach G. Helvetica Chimica Acta. 1952; 35:2344–2359.
90. Trotman-dickenson AF. J. Chem. Soc. 1949:1293–1297.
91. Leatherdale CA, Kagan CR, Morgan NY, Empedocles SA, Kastner MA, Bawendi MG. Phys. Rev. B. 2000; 62:2669–2680.

92. Luth H, Nyburg SC, Robinson PM, Scott HG. Mol. Cryst. Liq. Cryst. 1974; 27:337–357.
93. Chen O, Chen X, Yang Y, Lynch J, Wu H, Zhuang J, Cao YC. Angew. Chem., Int. Ed. 2008; 47:8638–841.
94. Yang YA, Wu H, Williams KR, Cao YC. Angew. Chem., Int. Ed. 2005; 44:6712–6715.
95. Cass LC, Malicki M, Weiss EA. Anal. Chem. 2013; 85:6974–6979. [PubMed: 23786216]
96. Bullen C, Mulvaney P. Langmuir. 2006; 22:3007–3013. [PubMed: 16548550]
97. Fernee MJ, Watt A, Warner J, Cooper S, Heckenberg N, Rubinsztein-Dunlop H. Nanotechnology. 2003; 14:991–997.
98. Dabbousi BO, Mikulec FV, Heine JR, Mattoussi H, Ober R, Jensen KF, Bawendi MG. J. Phys. Chem. B. 1997; 101:9463–9475.
99. Porter VJ, Geyer S, Halpert JE, Kastner MA, Bawendi MG. J. Phys. Chem. C. 2008; 112:2308–2316.
100. Shannon R. Acta Cryst. A. 1976; 32:751–767.
101. If instead, the covalent radius is used (Cd: 144 pm, Se: 120 pm), a 4 nm blue shift of the first excitonic peak is expected.
102. Tang J, Liu H, Zhitomirsky D, Hoogland S, Wang X, Furukawa M, Levina L, Sargent EH. Nano Lett. 2012; 12:4889–4894. [PubMed: 22881834]
103. Garcia-Rodriguez, R. l.; Hendricks, MP.; Cossairt, BM.; Liu, H.; Owen, JS. Chem. Mat. 2013; 25:1233–1249.
104. Gomez DE, van Embden J, Jasieniak J, Smith TA, Mulvaney P. Small. 2006; 2:204–208. [PubMed: 17193021]
105. Hanrath T, Veldman D, Choi JJ, Christova CG, Wienk MM, Janssen RAJ. ACS Appl. Mater. Interfaces. 2009; 1:244–250. [PubMed: 20353209]
106. Sun YG, Rogers JA. Adv. Mater. 2007; 19:1897–1916.
107. Tisdale WA, Williams KJ, Timp BA, Norris DJ, Aydil ES, Zhu XY. Science. 2010; 328:1543–1547. [PubMed: 20558714]
108. Yu D, Wang CJ, Wehrenberg BL, Guyot-Sionnest P. Phys. Rev. Lett. 2004; 92:216802. [PubMed: 15245304]
109. Zillner E, Fengler S, Niyamakom P, Rauscher F, Kohler K, Dittrich T. J. Phys. Chem. C. 2012; 116:16747–16754.
110. Guyot-Sionnest P, Shim M, Matranga C, Hines M. Phys. Rev. B. 1999; 60:R2181–R2184.
111. Jarosz M, Porter V, Fisher B, Kastner M, Bawendi M. Phys. Rev. B. 2004; 70:195327.
112. Jasieniak J, Califano M, Watkins SE. ACS Nano. 2011; 5:5888–5902. [PubMed: 21662980]
113. Law M, Luther JM, Song O, Hughes BK, Perkins CL, Nozik AJ. J. Am. Chem. Soc. 2008; 130:5974–5985. [PubMed: 18396872]
114. Lefrancois A, Couderc E, Faure-Vincent J, Sadki S, Pron A, Reiss P. J. Mat. Chem. 2011; 21:11524–11531.
115. Mentzel TS, Wanger DD, Ray N, Walker BJ, Strasfeld D, Bawendi MG, Kastner MA. Nano Lett. 2012; 12:4404–4408. [PubMed: 22784104]
116. Murphy JE, Beard MC, Nozik AJ. J. Phys. Chem. B. 2006; 110:25455–25461. [PubMed: 17165993]
117. Kutana A, Erwin SC. Phys. Rev. B. 2011; 83:235419.
118. Guyot-Sionnest P, Lhuillier E, Liu H. J. Chem. Phys. 2012; 137:154704. [PubMed: 23083181]
119. Koleilat GI, Levina L, Shukla H, Myrskog SH, Hinds S, Pattantyus-Abraham AG, Sargent EH. ACS Nano. 2008; 2:833–840. [PubMed: 19206479]
120. Luther JM, Beard MC, Song Q, Law M, Ellingson RJ, Nozik AJ. Nano Lett. 2007; 7:1779–1784. [PubMed: 17530913]
121. Luther JM, Law M, Beard MC, Song Q, Reese MO, Ellingson RJ, Nozik AJ. Nano Lett. 2008; 8:3488–3492. [PubMed: 18729414]
122. Nagpal P, Klimov VI. Nat. Commun. 2011; 2:486. [PubMed: 21952220]
123. Talapin DV, Murray CB. Science. 2005; 310:86–89. [PubMed: 16210533]

124. Talgorn E, Gao YN, Aerts M, Kunneman LT, Schins JM, Savenije TJ, van Huis MA, van der Zant HSJ, Houtepen AJ, Siebbeles LDA. Nat. Nano. 2011; 6:733–739.
125. Wehrenberg BL, Guyot-Sionnest P. J. Am. Chem. Soc. 2003; 125:7806–7807. [PubMed: 12822991]
126. Yu D, Wang CJ, Guyot-Sionnest P. Science. 2003; 300:1277–1280. [PubMed: 12764194]
127. Choi JJ, Lim YF, Santiago-Berrios MB, Oh M, Hyun BR, Sung LF, Bartnik AC, Goedhart A, Malliaras GG, Abruna HD, Wise FW, Hanrath T. Nano Lett. 2009; 9:3749–3755. [PubMed: 19719095]
128. Gao Y, Aerts M, Sandeep CSS, Talgorn E, Savenije TJ, Kinge S, Siebbeles LDA, Houtepen AJ. ACS Nano. 2012; 6:9606–9614. [PubMed: 23078408]
129. Kuo CY, Su MS, Ku CS, Wang SM, Lee HY, Wei KH. J. Mat. Chem. 2011; 21:11605–11612.
130. Liu Y, Gibbs M, Puthussery J, Gaik S, Ihly R, Hillhouse HW, Law M. Nano Lett. 2010; 10:1960–1969. [PubMed: 20405957]
131. Smith AR, Yoon W, Heuer WB, Baril SIM, Boercker JE, Tischler JG, Foos EE. J. Phys. Chem. C. 2012; 116:6031–6037.
132. Talgorn E, Moysidou E, Abellon RD, Savenije TJ, Goossens A, Houtepen AJ, Siebbeles LDA. J. Phys. Chem. C. 2010; 114:3441–3447.
133. Wolcott A, Doyeux V, Nelson CA, Gearba R, Lei KW, Yager KG, Dolocan AD, Williams K, Nguyen D, Zhu XY. J. Phys. Chem. Lett. 2011; 2:795–800.
134. Fafarman AT, Koh W.-k. Diroll BT, Kim DK, Ko D-K, Oh SJ, Ye X, Doan-Nguyen V, Crump MR, Reifsnyder DC, Murray CB, Kagan CR. J. Am. Chem. Soc. 2011; 133:15753–61.
135. Nag A, Kovalenko MV, Lee J-S, Liu W, Spokoyny B, Talapin DV. J. Am. Chem. Soc. 2011; 133:10612–10620. [PubMed: 21682249]
136. Zhitomirsky D, Furukawa M, Tang J, Stadler P, Hoogland S, Voznyy O, Liu H, Sargent EH. Adv. Mater. 2012; 24:6181–6185. [PubMed: 22968808]
137. Voznyy O. J. Phys. Chem. C. 2011; 115:15927–15932.
138. Hines MA, Scholes GD. Adv. Mater. 2003; 15:1844–1849.
139. Yu WW, Falkner JC, Shih BS, Colvin VL. Chem. Mat. 2004; 16:3318–3322.
140. Hassinen A, Moreels I, Donega CD, Martins JC, Hens Z. J. Phys. Chem. Lett. 2010; 1:2577–2581.
141. Leatherdale CA, Mikulec FV, Bawendi MG. J. Phys. Chem. B. 2002; 106:7619–7622.
142. Jasieniak J, Smith L, van Embden J, Mulvaney P, Califano M. J. Phys. Chem. C. 2009; 113:19468–19474.
143. Moreels I, Lambert K, Smeets D, De Muynck D, Nollet T, Martins JC, Vanhaecke F, Vantomme A, Delerue C, Allan G, Hens Z. ACS Nano. 2009; 3:3023–3030. [PubMed: 19780530]
144. Yu WW, Qu L, Guo W, Peng X. Chem. Mater. 2003; 15:2854–2860.
145. Kuznetsova NAK, O. L. Russ. Chem. Rev. 1992; 61:683.

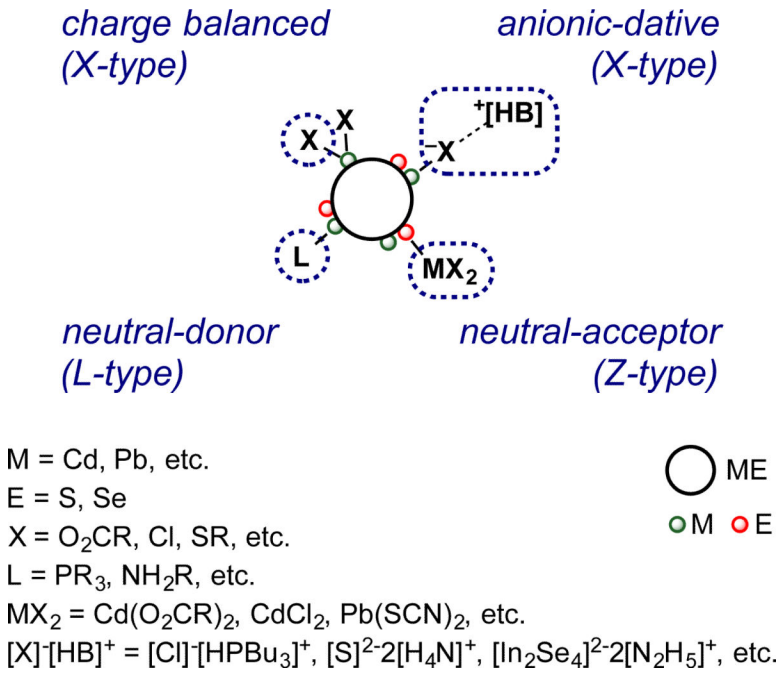

Scheme 1.

Nanocrystal ligand binding motifs as classified by the L,X,Z, formalism. Depictions of nanocrystal chemical formulas do not imply geometric structure.

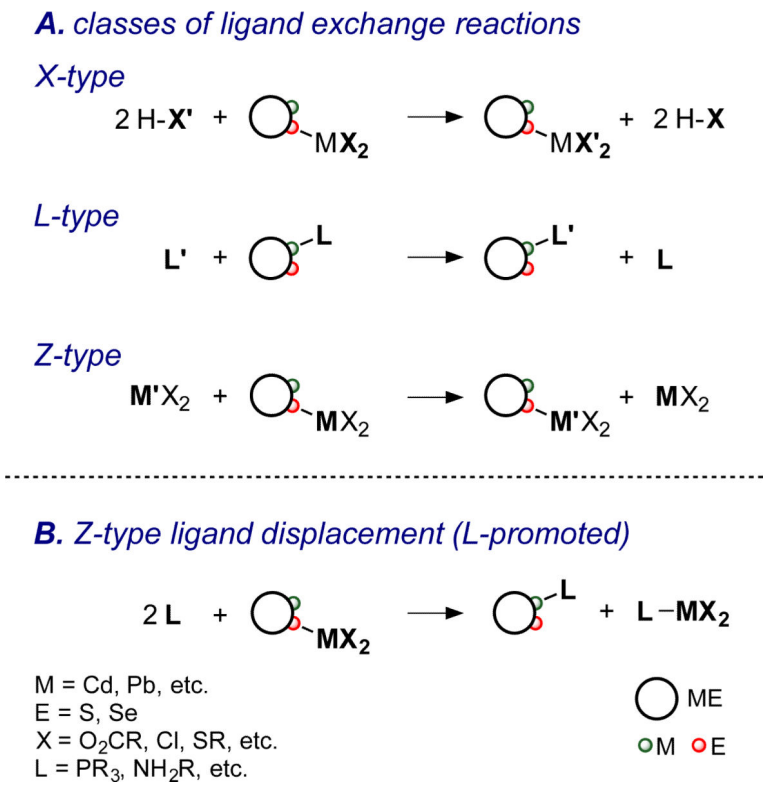

Scheme 2.

Example surface ligand modifications of metal chalcogenide nanocrystals including X-, L-, and Z-type exchange (**A**) and Z-type ligand displacement (**B**).

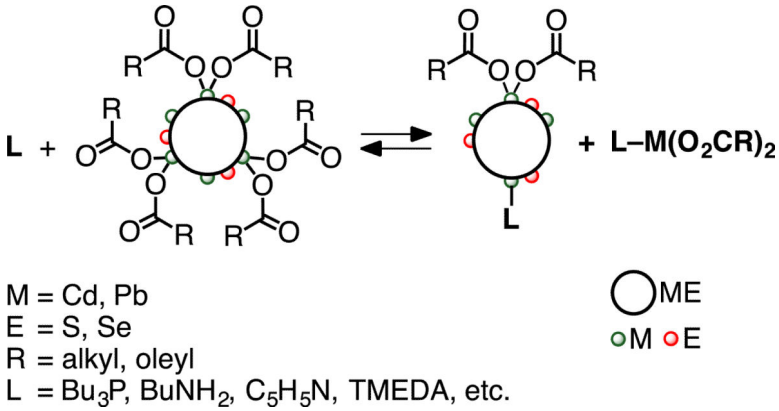

Scheme 3.

Displacement of L-M(O_2CR)$_2$ from metal chalcogenide nanocrystals promoted by L-type ligands. Depictions of nanocrystal chemical formulas do not imply geometric structure.

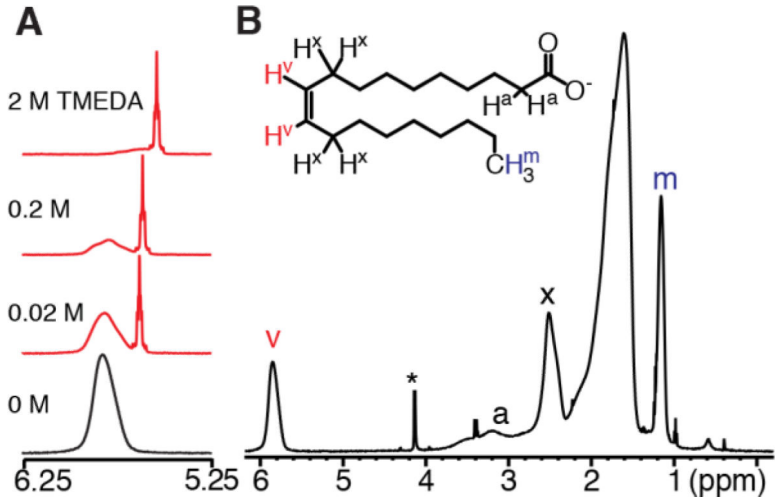

Figure 1.

(A) Vinyl region of the ^{1}H NMR spectrum of carboxylate-terminated CdSe nanocrystals shows displacement of $Cd(O_2CR)_2$ on treatment with increasing concentrations of TMEDA. (B) ^{1}H NMR spectrum of purified CdSe nanocrystals with chemical shift assignments. (*) Sharp signal at $\delta = 4.1$ ppm is ferrocene standard used to measure oleyl concentration (See Experimental). Changes to the chemical shifts of both free and bound signals at high concentration of TMEDA may be due to a change in the dielectric of the solvent medium. The final 2M concentration is ~20% by volume TMEDA. Similarly, as an increasing amount of $Cd(O_2CR)_2$ is removed from the nanocrystal, the density of aliphatic ligands changes as does their local dielectric medium.

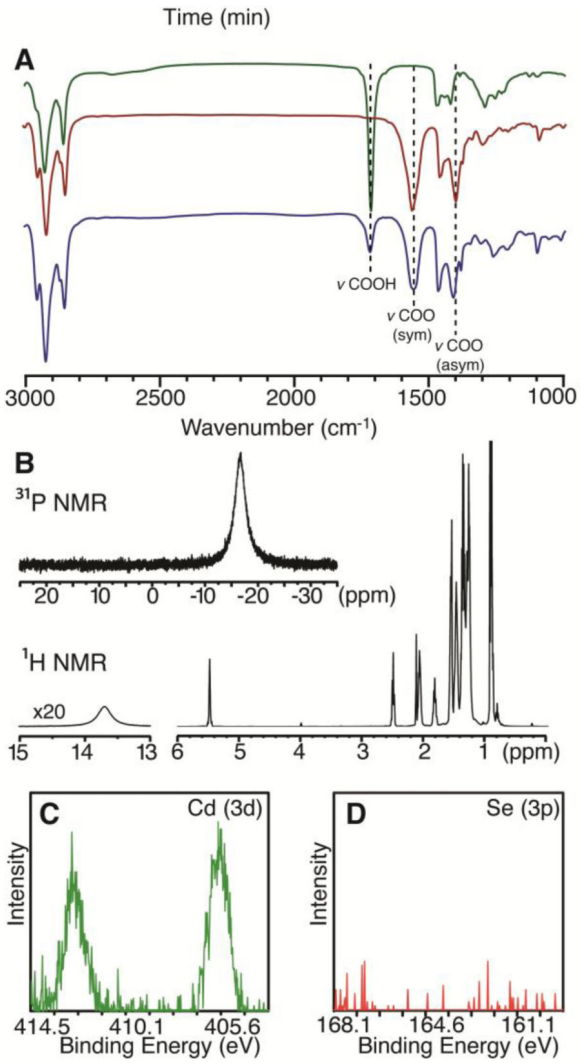

Figure 2.

(**A**) FT-IR spectra of $(Bu_3P)Cd(O_2CR)_2$ (R = oleyl and tridecyl) isolated from CdSe nanocrystals after exposure to Bu_3P (blue, bottom); an independently prepared cadmium oleate plus Bu_3P (red, middle); a mixture of oleic acid and Bu_3P (green, top). A small concentration of carboxylic acid 1720 cm^{-1} is present in the $(Bu_3P)Cd(O_2CR)_2$ isolated from nanocrystals (see below). (**B**) ^{31}P (top) and ^{1}H (bottom) NMR spectra of $(Bu_3P)Cd(O_2CR)_2$ (R = oleyl and tridecyl) isolated from CdSe nanocrystals. The broad resonance at $\delta = 13.7$ ppm has been magnified 20x and corresponds to an acid impurity (~8%). Top inset shows the ^{31}P chemical shift is downfield from the signal of free Bu_3P ($\delta = -17$ vs. −31 ppm). Furthermore, the resonance shifts further downfield as the concentration increses, perhaps due to the presence of cadmium complexes with multiple phosphine ligands in rapid exchange. Both the ratio of phospine and carboxylate signals in the ^{1}H NMR spectrum and the chemical shift of an authentic sample (Figure S4) indicate the isolated sample is a monophosphine complex. (**C**) Cadmium (*3d*) XPS spectrum of isolated $(Bu_3P)Cd(O_2CR)_2$. (**D**) XPS spectrum of $(Bu_3P)Cd(O_2CR)_2$ from the binding energy region characteristic of selenium (*3p*) shows no signal.

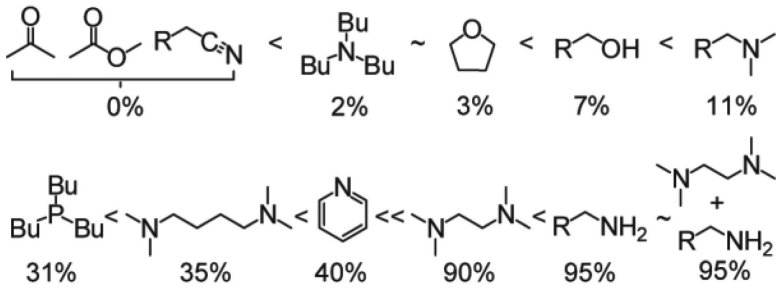

Scheme 4.

Relative displacement potency labeled with the percentage of L-Cd($O_2CR)_2$ displaced in a 2.0 M solution of the of L-type ligand.

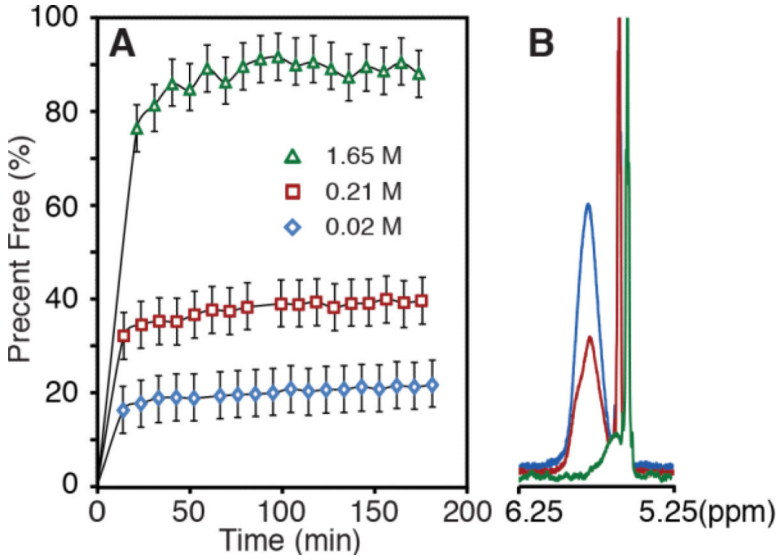

Figure 3.

(A) Temporal evolution of (κ^2-TMEDA)Cd(O_2CR)$_2$ displacement as measured by ^{1}H NMR spectroscopy at several concentrations of added TMEDA in d_6-benzene. (B) ^{1}H NMR spectra of the vinyl region after 200 minutes of reaction. Colors correspond to 0.02 M (blue, diamonds), 0.21 M (red, squares), and 1.65 M (green, triangles) TMEDA solutions. Error bars are set to 10% reflects error in the integration of ^{1}H NMR spectra (see experimental).

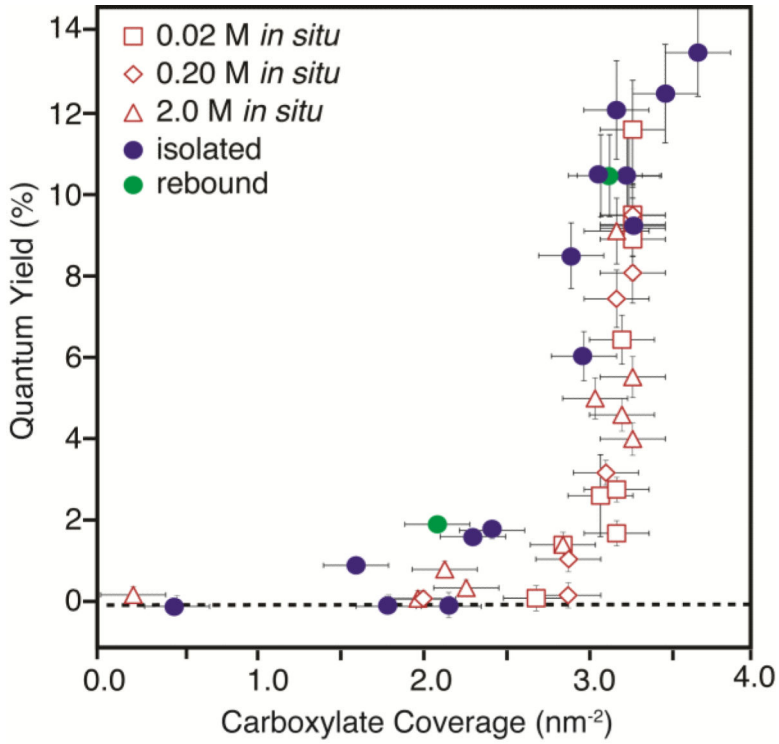

Figure 4.

Dependence of photoluminescence quantum yield on carboxylate coverage. Empty red shapes taken from *in situ* measurements using the neutral donors shown in Scheme 3. L-type ligands were added to a stock solution of CdSe nanocrystals (0.02 M in $^{-}O_2CR$) to a total concentration of 0.02 M (squares), 0.2 M (diamonds) and 2.0 M (triangles) (see experimental). Filled circles correspond to samples where the coverage was measured after isolation following displacement (blue) or rebinding (green) of $Cd(O_2CR)_2$. See supplemental for additional detail.

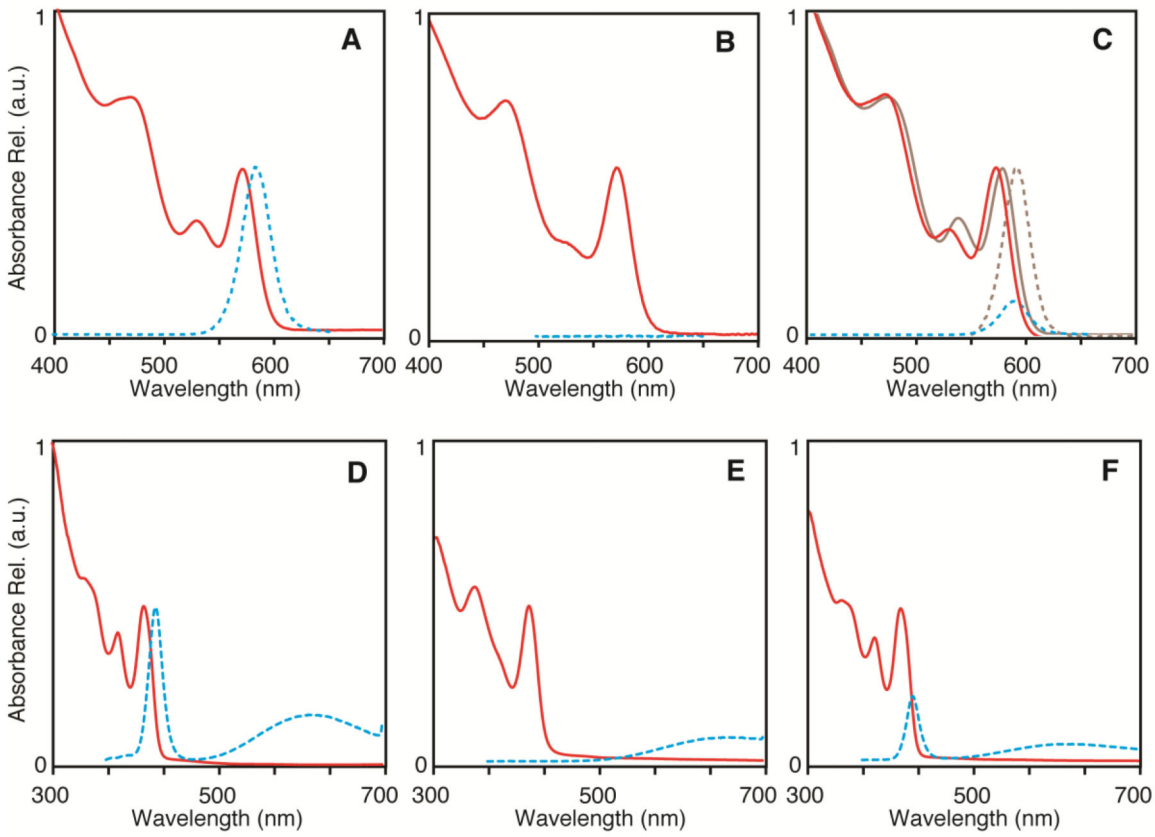

Figure 5.

Absorption (red, solid) and photoluminescence (blue, dashed) spectra of CdSe (A-C) and CdS (D-F) nanocrystals. CdSe nanocrystals: Purified after synthesis (A), isolated after treatment with TMEDA (B), and after rebinding $Cd(O_2CR)_2$ at room temperature (C). Gray spectra in Box C show absorption (solid) and photoluminescence (dashed) after heating at 240° C for 1 hr with added $Cd(O_2CR)_2$ and oleic acid. CdS nanocrystals: As synthesized, before purification (D), isolated after treatment with TMEDA (E), and after $Cd(O_2CR)_2$ rebinding at room temperature (F).

Table 1

Composition of Nanocrystals after isolation, displacement and rebinding of $M(O_2CR)_2$.

	Metal Chalcogenide	Treatment[a]	Diameter[b] (nm)	ME units per NC[c]	Ligands per NC[d]	Surface Ligand Density[e] (nm^{-2})
1a	**CdSe**	MeOAc	3.5	400(30)	160(30)	4.2(7)
1b	**CdSe**	**1b** + TMEDA/RNH_2	3.5	400(30)	10(2)/170(30)[f]	0.3(1)/4.5(8)[f]
2a	**CdSe**	MeOAc	3.6	430(40)	130(15)	3.3(5)
2b	**CdSe**	**2a** + TMEDA	3.6	430(40)	20(4)	0.6(1)
2c	**CdSe**	**2b** + $Cd(O_2CR)_2$[g]	3.6	430(40)	85(10)	2.1(4)
2d	**CdSe**	**2b** + Cd(O2CR)2[h]	3.8	520(50)	150(30)	3.3(6)
3a	**CdS**	TMEDA	4.0	670(110)	20(5)	0.4(1)
3b	**CdS**	**2a** + $Cd(O_2CR)_2$[g]	4.0	670(110)	40(10)	1.1(1)
4	**PbSe**	MeOAc	3.7	470(140)	135(15)	3.1(5)
5a	**PbS**	MeOAc	3.1	310(90)	130(15)	4.3(5)
5b	**PbS**	TMEDA	3.1	310(90)	75(10)	2.4(4)

[a] MeOAc: Isolated as reported in the Experimental; TMEDA/RNH_2: removal of $Cd(O_2CR)_2$ using 50:50 TMEDA/*n*-octylamine and isolation as described in the Experimental. TMEDA: removal of $Cd(O_2CR)_2$ using TMEDA and isolation as described in the Experimental. Cd(O2CR)2: addition of cadmium oleate followed by precipitation from THF using methyl acetate as described in the Experimental.

[b] Diameters are calculated from the energy of the lowest energy absorption according to refs. 129-132.

[c] ME (CdSe, CdS, PbSe, PbS) units per nanocrystal (NC) are calculated assuming a spherical shape and the molar volume of zincblende CdSe (17.80 nm^{-3}), zincblende CdS (20.09 nm^{-3}), rock salt PbS (19.12 nm^{-3}), and rock salt PbSe (17.39 nm^{-3}). Errors shown are propagated from the uncertainty in the diameter, which we estimate to be approximately one M-E bond distance (~0.2 nm).

[d] The number of organic ligands per nanocrystal (NC) is measured by comparing the concentration of ligands determined with ^1H NMR spectroscopy and the concentration of ME determined using absorption spectroscopy; (see experimental section for details).

[e] Ligand densities were calculated by dividing the number of ligands per nanocrystal by its surface area assuming a spherical shape.

[f] -O_2CR/RNH_2 coverages and densities. Coverage of RNH_2 is an upper limit as free and bound primary amines are in rapid exchange.

[g] room temperature

[h] 240 °C with added oleic acid (see Experimental)